Coherent structures in transitional pipe flow

Leo H. O. Hellström,[1, a)] Bharathram Ganapathisubramani,[2, b)] and Alexander J. Smits[3, c)]

[1)]*Mechanical and Aerospace Engineering, Princeton University, Princeton, NJ 08544, U.S.A.*

[2)]*Faculty of Engineering and the Environment, University of Southampton, Southampton, SO17 1BJ, U.K.*

[3)]*Mechanical and Aerospace Engineering, Princeton University, Princeton, NJ 08544, U.S.A., and Mechanical and Aerospace Engineering, Monash University, VIC 3800, Australia*

Transition to turbulence in pipe flow is investigated experimentally using a temporally resolved dual-plane particle image velocimetry (PIV) approach, at a Reynolds number of 3440. The flow is analyzed using proper orthogonal decomposition, and it is shown that the flow can be divided into two regions: a pseudo-laminar region governed by the presence of azimuthally steady traveling waves, and turbulent slugs. The evolution of the structures within the slugs is identified by using the temporally resolved data along with the dual-plane velocity field. These structures are shown to be remarkably similar to the large-scale-motions found in fully turbulent flows, with a streamwise and spatio-temporal extent about 4 pipe radii. The transition between structures are characterized by the detachment and decay of an old structure and the initiation of a new structure at the wall.

[a)]Email address for correspondence: lhellstr@Princeton.EDU

[b)]Email address for correspondence: G.Bharath@soton.ac.uk

[c)]Email address for correspondence: asmits@Princeton.EDU

I. INTRODUCTION

Pipe flow is linearly stable to small disturbances but non-linearly unstable to finite-amplitude disturbances, which makes it an abrupt process that immediately generates complex spatio-temporal flows[4]. This abrupt transition depends crucially on how the disturbances are brought to the system[3]. For example, Wu et al.[17] performed a direct numerical simulation of a transitional pipe flow and found that transition was sensitive to the disturbance magnitude and the critical Reynolds number, as well as the radial location at which the disturbance was introduced.

There has been significant progress in analyzing such flows by treating them as large dynamical systems. In this respect, exact solutions to the Navier-Stokes equations such as traveling waves and periodic orbits are of particular interest[6,13,15,16]. For instance, Schneider et al.[14] found that the global dynamical structure in pipe flow was dominated by a pair of strong counter-rotating vortices aligned along the streamwise axis, while Wedin and Kerswell[16] and Chantry et al.[4] examined the azimuthally decomposed structures and identified solutions for azimuthal mode numbers $m \in [1,6]$. These streamwise-averaged solutions bear many similarities to structures found in fully-developed turbulent pipe flow using azimuthally decomposed two-point correlations[5] and proper orthogonal decomposition (POD)[2,8,10], suggesting that the large-scale structures in transitional and fully turbulent pipe flow are intimately related.

These relationships were further investigated by Wu et al.[17], who found that the disturbances grew into small-scale hairpin packets or even large-scale-motions (LSM) that are typically found in fully turbulent flows[1]. They further showed that the hairpin packets grew into turbulent spots, supporting the observations by Wygnanski and Champagne[18] who found that the motions within turbulent spots (called slugs when occupying the entire cross-section of the pipe[12]) were similar to those in fully turbulent flows.

Hellström et al.[9] investigated experimentally such large-scale turbulence features in the cross-stream plane of a fully-developed turbulent pipe flow at a bulk Reynolds number $Re_D = 12,500$ using a POD procedure, and demonstrated that the gross features of the flowfield could be reconstructed using a relatively small number of energetically important POD modes. Hellström and Smits[8] and Hellström et al.[10] extended this approach by increasing the Reynolds number to 104,000, and azimuthally decomposing the flow field using a Fourier series expansion. They concluded that the dominant motions consist of three azimuthal and one radial structure. Hellström et al.[10] also showed that the extracted structures describe the hairpin packet or LSM with a span-

wise length defined by the azimuthal mode number, and that the radial evolution of the LSM was described by a "transition" between POD modes.

Here, we build on this previous body of work by using POD to identify energetically important structures in a transitional pipe flow within the turbulent slugs and within the pseudo-laminar regions surrounding the slugs. We also address the similarity of the structures found in a turbulent slug to those found in fully turbulent flows.

II. EXPERIMENTAL SETUP

The experiment was conducted using the same pipe flow facility and experimental techniques described by Hellström et al.[10]. The facility consist of seven glass pipe sections, and uses water seeded with 10μm glass hollow spheres as the working fluid. Approximately $180D$ downstream of the pipe entrance, the flow was simultaneously investigated in a cross-sectional plane and a streamwise plane using stereoscopic (2D-3C) and planar (2D-2C) particle image velocimetry (PIV), respectively. The streamwise plane was placed along the pipe centerline and centered on the cross-sectional plane, spanning a streamwise distance of $2.4D$.

The results presented here were obtained at a single Reynolds number $Re_D = U_b D/\nu = 3440$, where U_b is the bulk velocity, D is the pipe diameter ($= 2R$), and ν is the kinematic viscosity of water. All three PIV cameras were operated at 30 Hz, so that at $Re_D = 3440$ there was a bulk convective displacement of $0.15R$ between any two consecutive PIV snapshots. The full data set consisted of ten blocks, each containing 2200 image pairs, where each block represents a convective bulk velocity displacement of $418R$. The PIV data processing, including image processing, interpolation, and data validation techniques, were identical to that described by Hellström et al.[10]. The transition to turbulence was natural in the sense that there was no passive or active tripping device in place, and at this Reynolds number the flow was intermittently turbulent, alternating between turbulent slugs and approximately laminar regions, which we will refer to as pseudo-laminar regions.

III. PROPER ORTHOGONAL DECOMPOSITION

When performing POD, we consider only the fluctuating velocity field, which depends on the definition of the mean flow. In an intermittently turbulent flow, the time-averaged velocity profile

is sensitive to the occurrence rate of the slugs within each particular dataset. To circumvent this difficulty, we create a reference mean velocity profile for which we only use the average of the pseudo-laminar regions. These regions were selected such that the centerline velocity $U_{CL} > 1.8U_b$, while the slugs, or turbulent regions, were defined by $U_{CL} < 1.5U_b$. With these thresholds, approximately 18% of the data entries were considered to be in a turbulent region. Note that the reference profile does not follow precisely a parabolic shape.

Following Hellström et al.[11], we begin with a "direct" POD analysis of the three-component fluctuating velocity data in the cross-plane. We recap some of the definitions here to be sure of their meaning. The cross-correlation tensor only depends on the shift in the azimuthal (homogeneous) direction, and it can be shown to be a Fourier series. The eigenvalue problem becomes

$$\int_{r'} \mathbf{S}(m;r,r')\Phi^{(n)}(m;r')r'dr' = \lambda^{(n)}(m)\Phi^{(n)}(m;r), \tag{1}$$

where n represents the POD mode number, $\Phi^{(n)}$ are the radial eigenfunctions with the corresponding eigenvalues $\lambda^{(n)}$, and m represents the azimuthally decomposed mode number. The azimuthal decomposition has the benefit of making the analysis insensitive to the chosen mean flow, as all changes in mean flow are captured in $m = 0$ and can be discarded if desired. The time-averaged cross-correlation tensor, $\mathbf{S}$, is defined as

$$\mathbf{S}(m;r,r') = \lim_{\tau\to\infty} \frac{1}{\tau}\int_0^\tau \mathbf{u}_c(m;r,t)\mathbf{u}_c^*(m;r',t)dt, \tag{2}$$

where $\mathbf{u}_c$ denotes the three-component velocity field in the cross-sectional plane, and * denotes the conjugate transpose. The nature of the cylindrical coordinate system creates an asymmetry in the kernel with respect to r'. Glauser and George[7] addressed this issue by absorbing r' into the eigenfunctions and the cross-correlation tensor, creating a set of substitute equations which can be solved using Hilbert-Schmidt theory. The substitute functions are here denoted by an overbar,

$$\int_{r'} \overline{\mathbf{S}}(m;r,r')\overline{\Phi}^{(n)}(m;r')dr' = \lambda^{(n)}(m)\overline{\Phi}^{(n)}(m;r), \tag{3}$$

with the corresponding time-averaged cross-correlation tensor:

$$\overline{\mathbf{S}}(m;r,r') = \lim_{\tau\to\infty} \frac{1}{\tau}\int_0^\tau r^{1/2}\mathbf{u}_c(m;r,t)\mathbf{u}_c^*(m;r',t)r'^{1/2}dt. \tag{4}$$

At this point, each mode is subject to a phase shift such that their streamwise component is real. This procedure has no implication on its optimality but is solely a matter of azimuthally aligning

the modes with the streamwise plane when creating the dual-plane modes. The optimal POD modes can now be retrieved by

$$\Phi^{(n)}(m;r) = \overline{\Phi}^{(n)}(m;r)r^{-1/2}. \tag{5}$$

The presence of each mode at each instance in time can be identified by the POD (or random) coefficients $\alpha^{(n)}(m;t)$ which are determined by projecting the modes back onto the fluctuating velocity field,

$$\alpha^{(n)}(m;t) = \int_r r^{1/2}\mathbf{u}_c(m;r,t)\overline{\Phi}^{(n)^*}(m;r)dr. \tag{6}$$

In order to visualize the streamwise evolution of the POD modes, we create a dual-plane mode $\Psi^{(m,n)}(\theta,r,x)$. Instead of creating the dual-plane mode by a conditional average, as done by Hellström et al.[10], we create the mode by performing an inner-product between the POD coefficients and the dual-plane velocity field. That is,

$$\Psi^{(m,n)}(\theta,r,x) := \lim_{\tau\to\infty}\int_0^\tau \mathbf{u}_d(\theta,r,x,t)\Re\{\alpha^{(n)}(m;t)\}dt \tag{7}$$

where $\mathbf{u}_d$ represents the dual-plane velocity field. Because the streamwise component of each mode has been forced to be real, we reduce $\alpha^{(n)}$ to consider only its real part, and force $\Psi^{(m,n)}$ to align with the streamwise plane. This construction is similar to that used by Hellström et al.[10], but with the added benefit of being threshold independent.

The relative energy in the fluctuating velocity field for the first 15 azimuthal modes ($m \in [0,15]$) and five POD modes ($n \in [1,5]$) is displayed in figure 1(a). It can be seen that 75% of the energy is associated with mode $\Phi^{(1)}(0;r)$. However, this mode represent the deviation between the pseudo-laminar and turbulent mean velocity profiles, and is of limited interest in the present analysis. By removing the energy contribution from $\lambda^{(1)}(0)$, the relative energy distribution becomes as seen in figure 1(b), where $\lambda^{(1)}(1)$ contains 33.7% of the energy, $\lambda^{(1)}(2)$ contains 6.31%, while $\lambda^{(1)}(3)$ and $\lambda^{(1)}(4)$ both contain 3.44% of the energy.

The POD modes $\Phi^{(n)}(m;r)$ are reduced to radial profiles, one for each POD mode number (n) and azimuthal mode number (m) combination. The streamwise component of the radial profile for the first POD mode and azimuthal modes 1 through 5 are illustrated in figure 2(a), where the pipe wall is located at $y/R = 0$ and the centerline at $y/R = 1$. The POD modes bear a close resemblance to those found in fully turbulent pipe flow at $Re_D = 104,000$[10], where the structures approach the wall as the azimuthal mode number increases. The higher order POD modes $(n > 1)$ for azimuthal mode number $m = 3$ are seen in figure 2(b), where there are increasing number of radial structures

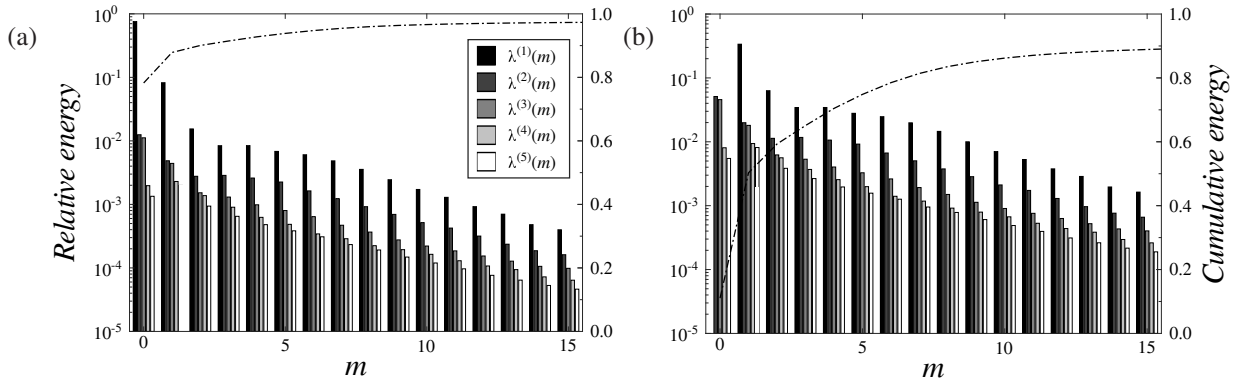

FIG. 1. The relative energy contribution of the first five POD modes ($n \in [1,5]$), with azimuthal modes $m \in [0,15]$. Cumulative energy content of the first five POD modes is represented by $-\cdot-$. (a) The complete set of eigenvalues ($\lambda^n(m)$), representing all deviation from the laminar flow field. (b) As in (a), but excluding the energy associated with the deviation of the laminar to turbulent mean velocity profile, resolved by $(n,m) = (1,0)$.

as n increases. The first three radial modes are similar to those found by Hellström et al.[10] while the modes $m = 3$ and $n \in \{4,5\}$ are mixed and can be represented as combinations of modes ($m = 3$, $n \in \{4,5\}$) obtained in the higher Reynolds number data.

For clarity, the modes in figure 2 can be reconstructed into two-dimensional modes that highlight their radial and azimuthal behavior. Figure 3(a) shows the reconstructed mode for $(m,n) = (1,1)$, which is similar to the exact traveling wave solution found by Wedin and Kerswell[16], while figure 3(b) through (d) represent $m = 3$ and $n \in \{1,2,3\}$. The streamwise component is shown using contours, while the in-plane components are visualized as streamlines. It can be seen that the streamwise and wall-normal velocity components display a strong negative correlation, making these structures major contributors to the Reynolds shear stress[8].

IV. TEMPORAL EVOLUTION

The presence of a turbulent slug was identified by the value of the instantaneous velocity at the centerline using a threshold $U_{CL} < 1.5U_b$. In figure 4(a), we show the scaled centerline velocity for data block 10, taken from the cross-plane. Although the turbulent slugs within the complete dataset vary in length by a factor of two, they all share the same gross features. The slug can be divided into three sections: (I) the head, from $tU_b/R \approx 100$ to ≈ 140, (II) the tail, located at

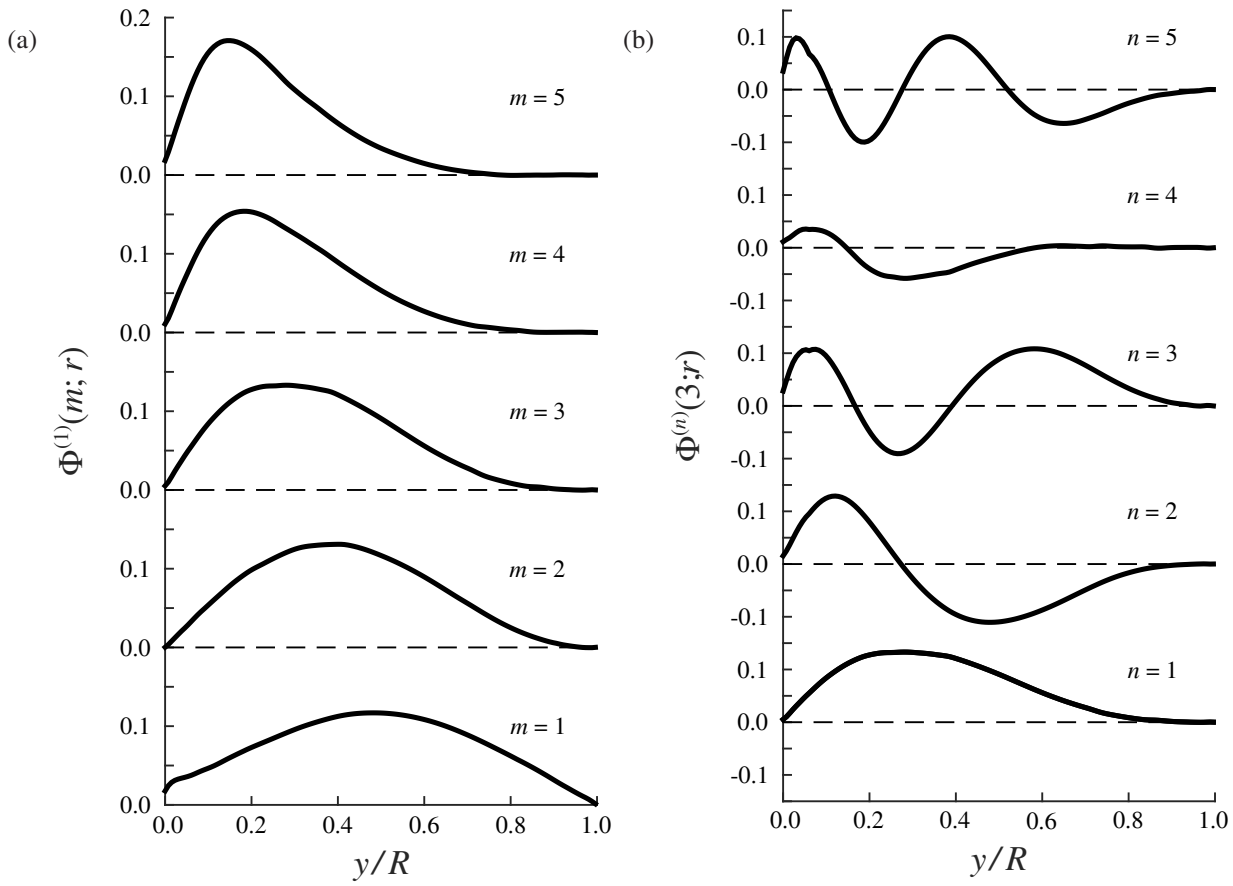

FIG. 2. Modal profile of the streamwise component of the POD modes. (a) First radial mode, $n = 1$, and $m \in [1,5]$. (b) Third azimuthal mode number, $m = 3$, and radial modes $n \in [1,5]$.

≈ 325, and (III) the flow in between, which resembles a turbulent-like flow[12]. It can further be seen that the centerline velocity between the slugs does not reach the laminar solution, $U_{CL}/U_b = 2$, but rather an approximation characteristic of the pseudo-laminar regime suggesting there is some modal activity causing these deviations.

The temporal activity of each mode can be viewed by the POD coefficients $\alpha^{(n)}(m;t)$, which are acquired by projecting each mode back onto the fluctuating velocity field. The coefficients are complex and carry magnitude and azimuthal phase information. In figure 4(b), we show the magnitude of the POD coefficients of the first POD modes, and azimuthal mode numbers $m \in [1,4]$, for data block 10. We note that the average value of $\alpha^{(1)}(1;t)$ in the slug is similar to that in the pseudo-laminar region, with the difference that it displays larger magnitude fluctuations while in the slug. The azimuthal phase of modes $n = 1$ and $m \in [1,2]$ are shown in figure 4(c). Both $\Phi^{(1)}(1;r)$ and $\Phi^{(1)}(2;r)$ describe azimuthally steady traveling waves with constant magnitude

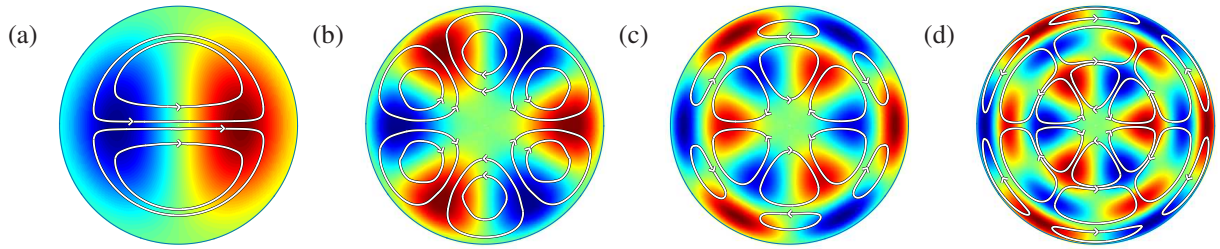

FIG. 3. Contour plots of the streamwise component of sample POD modes. Red represents positive and blue negative modal values, respectively. The streamlines indicate the in-plane components of the POD modes, $\Phi^{(n)}(m;r)$. (a) $\Phi^{(1)}(1;r)$; (b) $\Phi^{(1)}(3;r)$; (c) $\Phi^{(2)}(3;r)$; (d) $\Phi^{(3)}(3;r)$.

while in the pseudo-laminar regions, with a length scale $> 100R$. The two modes alternate phase from one pseudo-laminar region to another, such that its mean value is zero. The higher order azimuthal modes $(m \geq 3)$ are present only within the slug.

In the centerline region, the slug tail travels at a slower speed than the pseudo-laminar fluid behind it, hence compressing the tail. This can be seen by the sharp increase in centerline velocity and also by the high modal activity during the tail, followed by an almost complete decay afterwards. However, while in a turbulent slug, as in fully turbulent flow, mode $\Phi^{(1)}(3;r)$ is one of the most energetic modes after $\Phi^{(1)}(1;r)$.

To estimate the temporal evolution between the resolved POD mode, we create the normalized cross-correlation ρ, defined as:

$$\rho(m_1,n_1,m_2,n_2,\tau) := \frac{\left(\alpha^{(n_1)}(m_1;t),\alpha^{(n_2)}(m_2;t+\tau)\right)}{\|\alpha^{(n_1)}(m_1;t)\|\|\alpha^{(n_2)}(m_2;t)\|}, \tag{8}$$

where $(\cdot,\cdot)$ is the sliding inner-product with respect to time, and $\|\cdot\|$ represents its L^2-norm[10]. Figure 5 shows the magnitude of the cross-correlations between the reference mode, $\Phi^{(1)}(3;r)$, and for the first three POD modes $(n \in [1,3])$ and azimuthal modes $m \in [1,4]$. We choose $\Phi^{(1)}(3;r)$ to be the reference mode as it is the most energetic mode within the turbulent slug. It can be seen in figure 5 that the modes stays correlated with modes resolved by the same azimuthal mode number. Furthermore, the largest correlation values for the cross-correlation with the higher order POD mode have a temporal offset, where the peak for $n = 2$ is located about one convective radius downstream, and about 2 radii for $n = 3$, suggesting that the temporal evolution of mode $\Phi^{(1)}(3;r)$ is through modes $\Phi^{(2)}(3;r)$ and $\Phi^{(3)}(3;r)$.

These correlations, together with the POD modes, are now used to create a spatio-temporal

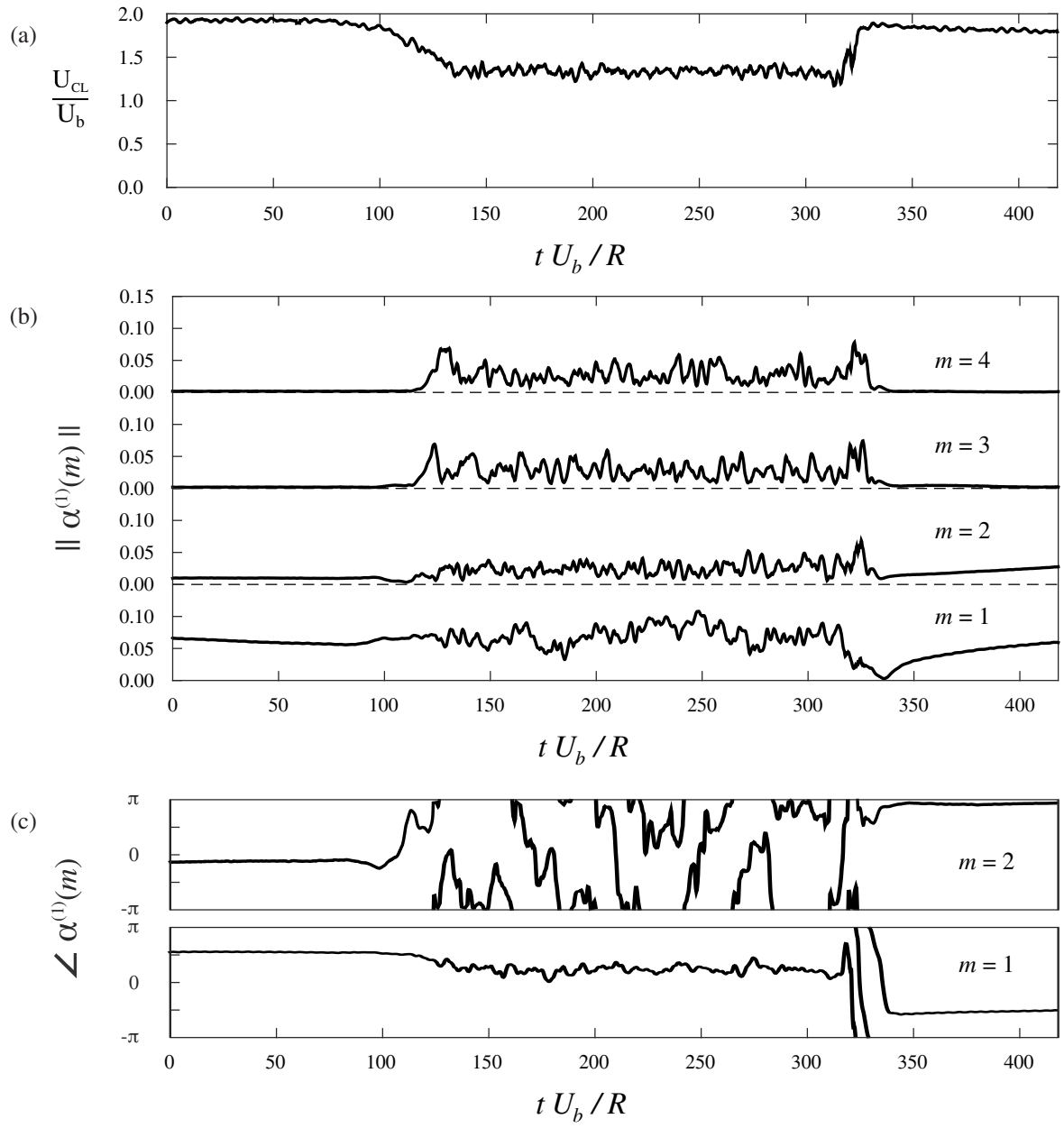

FIG. 4. Temporal activity of the flow field for data block 10. (a) Scaled centerline velocity. (b) Magnitude of POD coefficients $\alpha^{(1)}(1;t)$ for $n = 1$ and $m \in [1,4]$. (c) Azimuthal phase of POD coefficients $\alpha^{(1)}(1;t)$ for $n = 1$ and $m \in [1,2]$.

structure. We consider only azimuthal mode $m = 3$ and the first five POD modes shown earlier in figure 2(b). The structure is constructed by superimposing the product between the correlation values and the corresponding POD modes, that is, $\sum_n \rho(3,1,3,n,\tau)\Phi^{(n)}(3;r)$. The resulting structure is displayed in figure 6, where we have isolated a single positive structure using an isosurface corresponding to 50% of the maximum value. The correlation ρ is complex and it allows for any

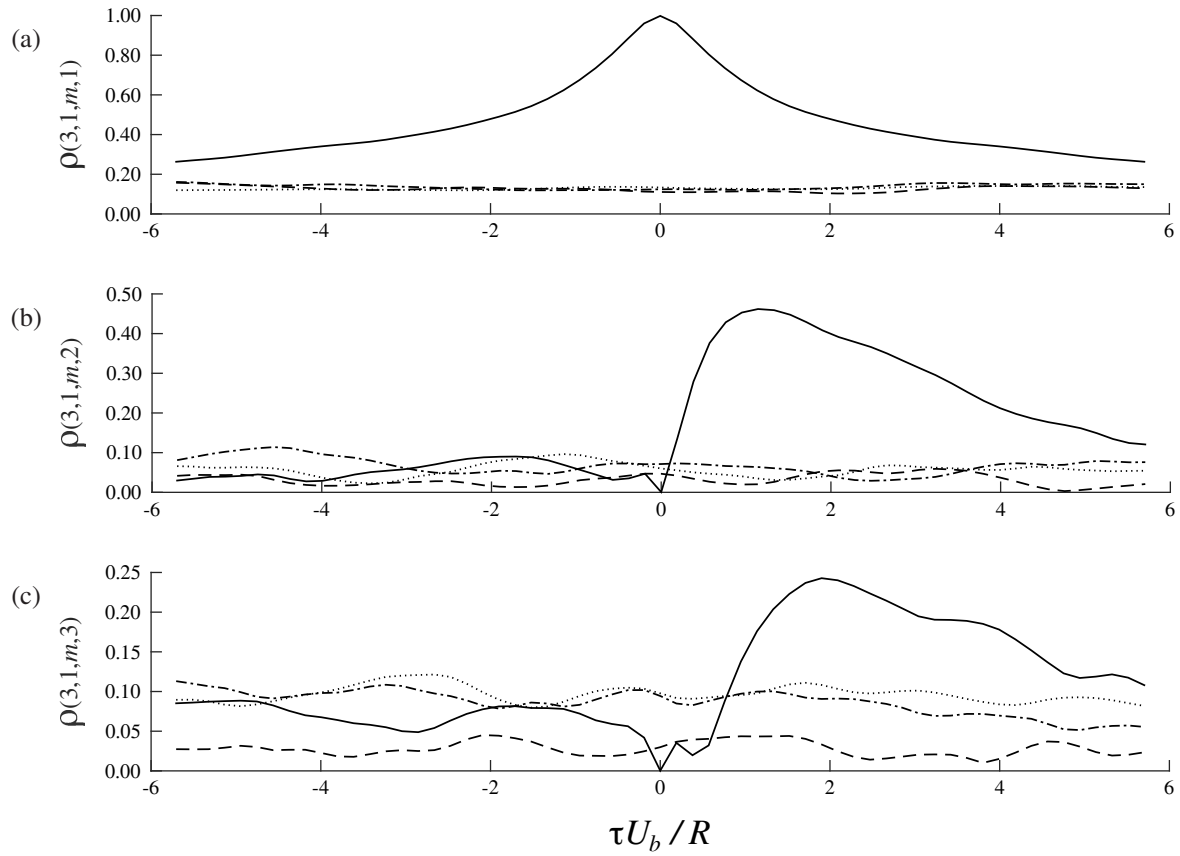

FIG. 5. Magnitude of the cross-correlation of the reference POD coefficient $\alpha^{(1)}(3;t)$ and the coefficients spanning, $m \in [1,4]$ and $n \in [1,3]$. (a) shows the correlation between the reference mode and $\alpha^{(1)}(m;t)$; (b) $\alpha^{(2)}(m;t)$; (c) $\alpha^{(3)}(m;t)$. The time step offset has been scaled using the bulk velocity and pipe radius. $\cdots$ represents $m = 1$; $\cdot - \cdot$ represents $m = 2$; — represents $m = 3$; $- - -$ represents $m = 4$.

azimuthal rotation, but as this is a statistical structure any rotation is expected to average to zero, as seen in figure 6(b). In a similar manner, since modes $n \in \{2,3\}$ describe the front end of the structure, modes $n \in \{4,5\}$ resolve the downstream end. The figure indicate a structure governed by a radial evolution, very similar to the large-scale-motions found in fully turbulent flows. Here, the structure is initiated at the wall, then grows radially, detaches from the wall, and finally decays.

V. DUAL-PLANE MODES

The spatio-temporal structures suggest strong similarities between the turbulence in a slug and that in fully turbulent pipe flow. To examine these similarities further, without being limited by the temporal resolution of the PIV system, we use the dual-plane modes, $\Psi^{(m,n)}(\theta,r,x)$, defined

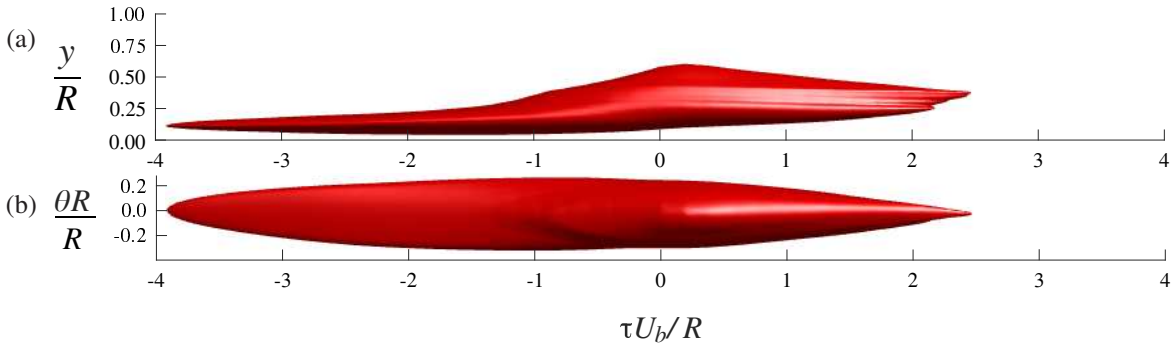

FIG. 6. Isosurface of an isolated spatio-temporal structure for $m = 3$ and $n \in [1,5]$. The isosurface value is chosen to be +50% of the maximum value. (a) side view; (b) seen from pipe centerline. Flow is from left to right.

by equation 7. The modes were constructed using three datasets: the current dataset acquired at $Re_D = 3440$, a dataset at $Re_D = 51,700$ from Hellström et al.[11], and a dataset at $Re_D = 104,000$ from Hellström et al.[10]. The two latter datasets were re-analyzed according to the procedure in section III.

The streamwise components of the dual-plane modes are shown in figure 7, where the left column shows mode $\Psi^{(3,1)}$ and the right column shows mode $\Psi^{(3,3)}$. The top, middle and bottom rows show the modes for $Re_D = 3440$, $Re_D = 51,700$ and $Re_D = 104,000$, respectively. The left column in figure 7 shows the initial structures which remain attached to the wall while growing in size, extending well into the wake region. The structure shows a generally similar behavior for this range of Reynolds numbers and is about $4R$ long, although the streamwise correlation for the structure within the slug flow is somewhat weaker. As previously reported by Hellström et al.[10], and illustrated in figure 5, mode $\Psi^{(3,1)}$ is followed by a "transitional mode" describing its evolution: $\Psi^{(3,2)}$ and $\Psi^{(3,3)}$, which shows the transition between subsequent structures. The right column shows mode $\Psi^{(3,3)}$, which identifies a ramp-like structure where the downstream end is detached from the wall. As the structure detaches, a new structure of the same sign is initiated at the wall, with an opposite signed structure in between. The length of the intermediate structure varies between the different datasets, from being about $2R$ in figure 7(b) to about R in figure 7(f). The detachment of the structure is rapid, occurring over a distance of about one radius, with an evolution very similar to the growth of the LSMs described by Adrian et al.[1].

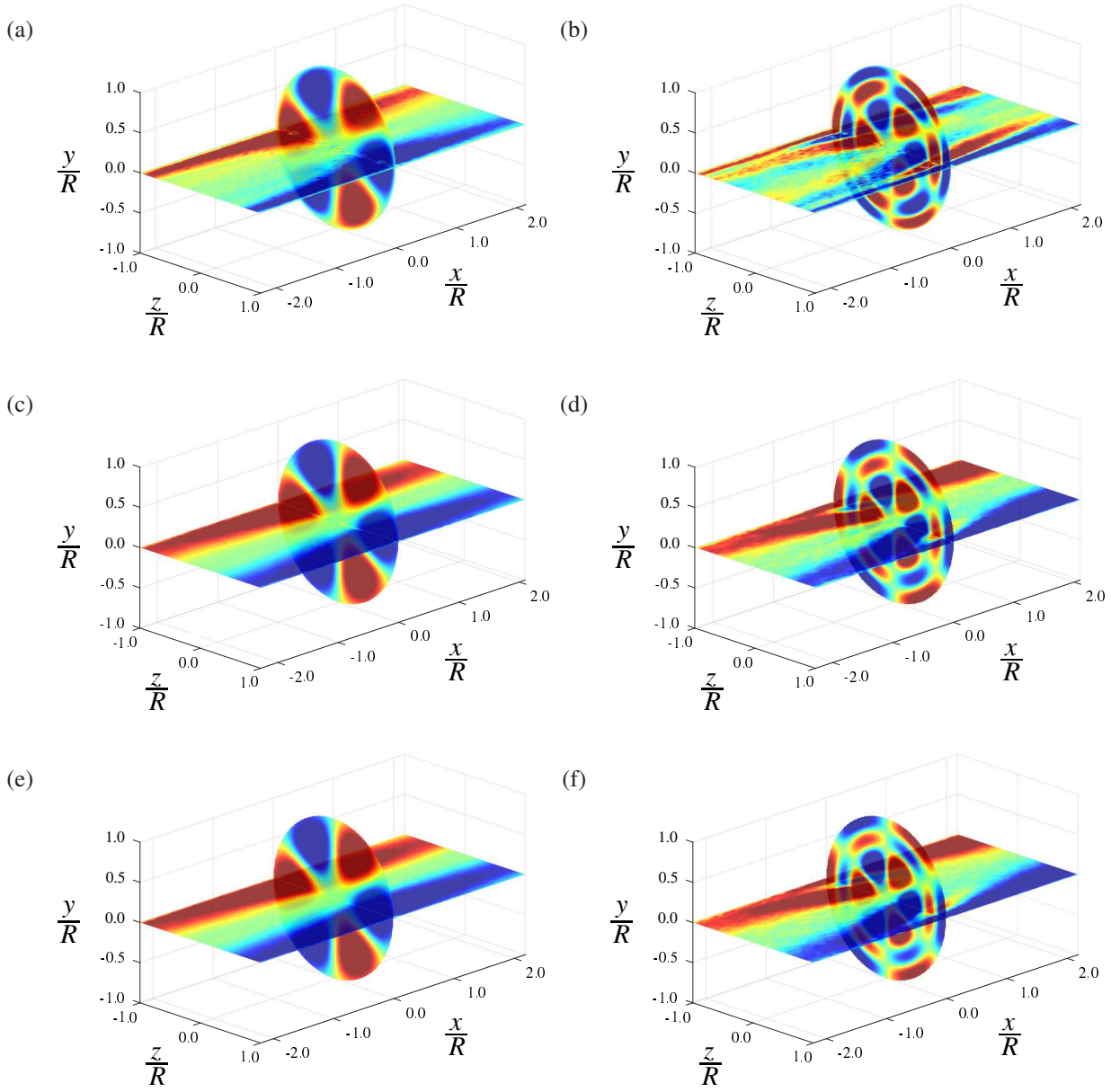

FIG. 7. Streamwise components of the dual-plane modes $\Psi^{(m,n)}(\theta,r,x)$. (a) $\Psi^{(3,1)}$ and (b) $\Psi^{(3,3)}$ at $Re_D = 3440$. (c) $\Psi^{(3,1)}$ and (d) $\Psi^{(3,3)}$ at $Re_D = 51,700$. (e) $\Psi^{(3,1)}$ and (f) $\Psi^{(3,3)}$ at $Re_D = 104,000$. Flow goes from left to right.

VI. DISCUSSION AND CONCLUSIONS

The transitional pipe flow at $Re_D = 3440$ was divided into two parts, a pseudo-laminar and a turbulent part. The structures in the pseudo-laminar part were governed by azimuthally steady traveling waves resolved by the lower order azimuthal POD modes, in particular modes $n = 1$ and

$m \in \{1,2\}$. These modes alter the azimuthal phase from opposite sides of a turbulent slug, such that their mean is zero. It is also the presence of these modes that prevents the velocity profile from fully recovering to a parabolic profile.

The turbulent parts (slugs) were composed of the lower order azimuthal modes which were present in the laminar regions ($m \leq 2$), with the addition of the higher order azimuthal modes ($m \geq 3$). The most energetic structures within the slugs were those associated with azimuthal mode numbers $m \in \{3,4\}$, where the POD modes show a strong resemblance to those found in fully turbulent pipe flow.

The form of the structures within the turbulent slugs themselves were shown to be similar to the large-scale-motions found in fully turbulent flows. These structures were characterized by a streamwise and temporal extent of about $4R$, after which a transition to a new structure occurred. The transition between structures was characterized by the detachment and decay of an old structure and the initiation of a new structure at the wall. The gross features of these organized motions were found to be insensitive to Reynolds number, and the structures within a slug were remarkably similar to those in a fully turbulent pipe flows at $Re_D = 51,700$ and $Re_D = 104,000$.

This work was supported under ONR Grant No. N00014-15-1-2402 (Program Manager Ron Joslin). BG gratefully acknowledges the support from European Research Council (ERC Grant agreement no 277472).

REFERENCES

[1]R. J. Adrian, C. D. Meinhart, and C. D. Tomkins. Vortex organization in the outer region of the turbulent boundary layer. *J. Fluid Mech.*, 422:1–54, 2000.

[2]J. R. Baltzer, R. J. Adrian, and X. Wu. Structural organization of large and very large scales in turbulent pipe flow simulation. *J. Fluid Mech.*, 720:236–279, 2013.

[3]S. Bottin, F. Daviaud, P. Manneville, and O. Dauchot. Discontinuous transition to spatiotemporal intermittency in plane Couette flow. *EPL (Europhysics Letters)*, 43(2):171, 1998.

[4]M. Chantry, A. P. Willis, and R. R. Kerswell. Genesis of streamwise-localized solutions from globally periodic traveling waves in pipe flow. *Phys. Rev. Lett.*, 112(16):164501, 2014.

[5]D. J. C. Dennis and F. M. Sogaro. Distinct organizational states of fully developed turbulent pipe flow. *Phys. Rev. Lett.*, 113:234501, 2014.

[6]H. Faisst and B. Eckhardt. Traveling waves in pipe flow. *Phys. Rev. Lett.*, 91(22):224502, 2003.

[7]M. N. Glauser and W. K. George. Orthogonal decomposition of the axisymmetric jet mixing layer including azimuthal dependence. In *Advances in Turbulence*, pages 357–366. Springer, 1987.

[8]L. H. O. Hellström and A. J. Smits. The energetic motions in turbulent pipe flow. *Phys. Fluids*, 26(12):125102, 2014.

[9]L. H. O. Hellström, A. Sinha, and A. J. Smits. Visualizing the very-large-scale motions in turbulent pipe flow. *Phys. Fluids*, 23:011703, 2011.

[10]L. H. O. Hellström, B. Ganapathisubramani, and A. J. Smits. The evolution of large-scale motions in turbulent pipe flow. *J. Fluid Mech.*, 779:701–715, 2015.

[11]L. H. O. Hellström, I. Marusic, and A. J. Smits. Self-similarity of the large-scale motions in turbulent pipe flow. *J. Fluid Mech.*, 0:00–00, 2016.

[12]T. Mullin. Experimental studies of transition to turbulence in a pipe. *Annu. Rev. Fluid Mech.*, 43:1–24, 2011.

[13]O. Ozcakir, S. Tanveer, P. Hall, and E. A. II Overman. Travelling wave states in pipe flow. *Journal of Fluid Mechanics*, 791:284–328, 3 2016. ISSN 1469-7645. doi:10.1017/jfm.2015.751. URL `http://journals.cambridge.org/article_S002211201500751X`.

[14]T. M. Schneider, B. Eckhardt, and J. A. Yorke. Turbulence transition and the edge of chaos in pipe flow. *Phys. Rev. Lett.*, 99(3):034502, 2007.

[15]F. Waleffe. Three-dimensional coherent states in plane shear flows. *Phys. Rev. Lett.*, 81(19): 4140, 1998.

[16]H. Wedin and R. R. Kerswell. Exact coherent structures in pipe flow: travelling wave solutions. *J. Fluid Mech.*, 508:333–371, 2004.

[17]X. Wu, P. Moin, R. J. Adrian, and J. R. Baltzer. Osborne Reynolds pipe flow: Direct simulation from laminar through gradual transition to fully developed turbulence. *Proceedings of the National Academy of Sciences*, 112(26):7920–7924, 2015.

[18]I. J. Wygnanski and F. H. Champagne. On transition in a pipe. Part 1. The origin of puffs and slugs and the flow in a turbulent slug. *J. Fluid Mech.*, 59(02):281–335, 1973.